International Journal of Heat and Mass Transfer 54 (2011) 1572–1577

Contents lists available at ScienceDirect

International Journal of Heat and Mass Transfer

journal homepage: www.elsevier.com/locate/ijhmt

Single bubble dynamics on a superhydrophilic surface with artificial nucleation sites

Youngsuk Nam [a], Eduardo Aktinol [a], Vijay K. Dhir [a], Y. Sungtaek Ju [a,b,*]

[a] University of California, Mechanical and Aerospace Engineering Department, 420 Westwood Plaza, Los Angeles, CA 90095-1597, USA
[b] California NanoSystems Institute (CNSI), UCLA, USA

ARTICLE INFO

Article history:
Received 7 January 2010
Received in revised form 11 November 2010
Accepted 11 November 2010
Available online 21 December 2010

Keywords:
Single bubble
Superhydrophilic
Cupric oxide
Bubble departure diameter

ABSTRACT

The dynamics of single bubbles on a superhydrophilic surface with well-defined nucleation sites are studied. The superhydrophilic surfaces are prepared by forming CuO nanostructures on a silicon substrate with an isolated microcavity. The bubble departure diameter in water is observed to be 2.5 times smaller and the growth period 4 times shorter on the superhydrophilic surface than on a silicon substrate. A model balancing the buoyancy with the surface tension force captures the departure diameter well, confirming the importance of wettability on bubble dynamics. The present work helps develop new surfaces for controlled phase change heat transfer and bubble-based micro-devices.

1. Introduction

Fundamental understanding of bubble nucleation and growth on heated surfaces is essential for developing mechanistic models of boiling heat transfer and designing bubble-driven micro-devices. Surface wettability has long been identified as one of the important factors affecting bubble growth and departure dynamics [1]. Previous studies reported significant increases in the critical heat flux for pool boiling [2] and water jet impingement cooling [3] on superhydrophilic surfaces with apparent contact angles <10°. Significant enhancement in the critical heat flux of pool boiling in nanofluids has been also attributed to the improved wettability caused by nanoparticle deposition [4,5]. Although such enhancements may perhaps be viewed as intuitive, detailed understanding of their exact mechanisms is still lacking.

Studies of bubble dynamics on well-defined isolated nucleation sites have served useful roles in elucidating bubble dynamics and facilitating the development and validation of numerical models [6,7]. Past experimental studies of single or quasi-single bubble dynamics used well-wetting liquids, such as FC-72, or added surfactants to investigate the effects of surface wettability on bubble dynamics [1,8] and pool boiling heat transfer [9,10].

We extend these previous studies and report our experimental and numerical study of single bubble dynamics on superhydrophilic surfaces using water, which has very different thermophysical and interfacial properties than well-wetting organic liquids. Our results enable quantitative assessment of the validity of existing correlations for the bubble departure characteristics. Combined with our demonstrated surface modification scheme, the present work helps develop new micro/nano-structured surfaces for advanced boiling applications.

2. Sample preparation

The static contact angle of water droplets on air-exposed Cu surfaces often exceeds 70°. Previous studies [2,3] applied TiO_2 coating to enhance the wettability of Cu surfaces, but the TiO_2 layers gradually lost their superhydrophilicity in the absence of UV irradiation [11]. In the present work, a controlled chemical oxidation is used to form superhydrophilic CuO nanostructures on a Cu film [12]. It is well-established that solid surfaces with appropriate combinations of the surface energy and morphology exhibit extreme wettability [13,14].

We first microfabricate isolated cylindrical cavities to serve as artificial bubble nucleation sites on prime-grade silicon substrates. Organic residues are first removed by dipping the substrates for 10 min in a Piranha (H_2SO_4:H_2O_2 = 4:1) solution followed by rinsing in filtered deionized water and nitrogen gas blow drying. The microcavities are formed using a deep reactive ion etching (DRIE) technique through a photoresist (AZ 5214) mask. After the DRIE process, the photoresist layer is stripped using acetone and O_2 plasma etching.

A 1 μm-thick Cu film is subsequently deposited using e-beam evaporation. The sample is immersed in an aqueous mixture of $NaClO_2$, NaOH, and $Na_3PO_4 \cdot 12H_2O$ at 95 °C for 5 min to form CuO nanostructures on the film [12]. Fig. 1(b) shows scanning

* Corresponding author at: University of California, Mechanical and Aerospace Engineering Department, 420 Westwood Plaza, Los Angeles, CA 90095-1597, USA. Tel.: +1 310 825 0985; fax: +1 310 206 2302.
E-mail address: just@seas.ucla.edu (Y.S. Ju).

0017-9310/$ - see front matter © 2010 Elsevier Ltd. All rights reserved.
doi:10.1016/j.ijheatmasstransfer.2010.11.031

Nomenclature

D	bubble diameter (m)
D_d	bubble departure diameter (m)
D_0	characteristic diameter (m)
d	diameter (mm)
F	force (N)
g	gravitational acceleration (m/s^2)
h	height (mm)
l_0	characteristic length (m)
P	pressure (Pa)
Re	Reynolds number
t	time (s)
t_0	characteristic time (s)
T	temperature (K)
u	velocity (m/s)
u_0	characteristic velocity (m/s)
w	diameter of cavity (μm)

Greek symbols

φ	apparent contact angle (deg)
σ	surface tension (N/m)
ρ	density (kg/m^3)

Subscripts

B	buoyancy
c	cavity
D	drag
I	inertia
l, v	liquid and vapor phase
S	surface tension
sub	subcooling
w	wall

electron microscopy (SEM) images of the isolated microcavity surrounded by the nanostructured Cu film. Since the oxidation process is quasi-self limiting [12], we can form very uniform nanostructures over large surface areas. The static contact angle of water droplets (~4 μL) measured over five different spots on the 100-mm diameter sample is 7.5 ± 2°.

We leave the inner wall of the cavity uncovered with the CuO nanostructures by exploiting the directionality of the thin-film deposition process. Trapped gas inside the cavity decreases the superheat required for the onset of heterogeneous nucleation (Fig. 1(a)) and allows the cavity to serve as an effective artificial bubble nucleation site [15].

To be consistent with previous single bubble experiments conducted using water [1,7,8,16,17], we set the cavity diameter (w) at 15 μm. We do not expect small changes in the cavity diameter to affect the bubble growth dynamics and departure diameter as the bubble contact line quickly extends beyond the periphery of the cavity. Bubble departure is affected mostly by the surrounding flat superhydrophlic surface.

The depth of the cavity should be larger than $w/\tan\varphi$ to facilitate the gas entrapment (Fig. 1(a)). We estimate the contact angle of the cavity inner wall to be approximately 20–40° from the measured contact angles of water droplets on flat silicon surfaces that experienced comparable DRIE processes. We set the cavity depth at 70 μm for the present sample and confirm that the cavity serves as an effective bubble nucleation site.

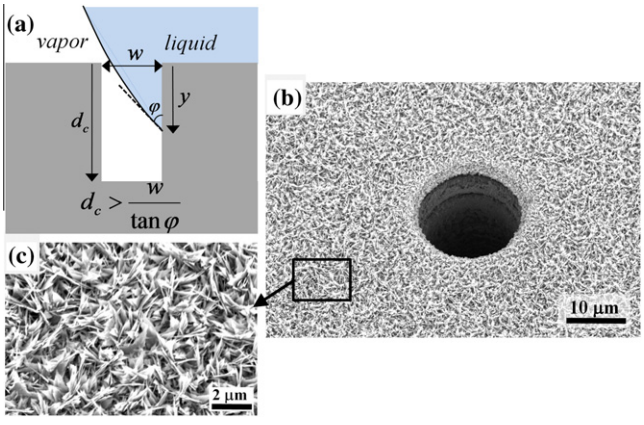

Fig. 1. (a) Schematic representation of vapor entrapment in a microcavity. (b) and (c) SEM images of the isolated cylindrical microcavity surrounded by the nanostructured Cu film (b) and the CuO nanostructures (c).

3. Experimental setup and procedure

Pool boiling experiments are conducted using an experimental setup discussed in our earlier publication [16]. Briefly, the setup consists of a polycarbonate test chamber (d = 200 mm, h = 93 mm), a quartz window (d = 50.8 mm), and a base plate. Two cartridge heaters are immersed in the liquid to control the sub-cooling level. The entire chamber is thermally insulated with melamine foam layers. A high speed camera (Fastcam MC2, Photron) equipped with a zoom lens (105 mm f/2.8D AF Micro Nikkor) is used to capture video images of bubbles.

The wettability of the heating surfaces is characterized through *in situ* contact angle measurements, supplemented by static contact angle measurements [18]. Sequential video frames obtained over multiple bubble ebullition cycles are analyzed using image analysis software [19]. To measure the static contact angle, a droplet (~4 μL) of filtered de-ionized water is placed on the sample surface and its shape is captured and analyzed using a goniometer (First Ten Angstroms (FTÅ) 4000) [18,20]. Measurements are performed at five different spots on the sample and the experiments are repeated three times at each spot. The resulting fifteen contact angle values are averaged and the mean value is reported together with the standard deviation.

Uncontrolled bubble nucleation over areas surrounding the artificial cavity can block an optical view and make a direct observation of single bubble dynamics difficult. Since such undesired bubble nucleation is effectively suppressed on our samples, we can make the lateral dimensions of our chamber much larger than the expected bubble diameters. This helps avoid any unintended wall effects and also allows the use of very low subcooling levels. These represent key differences from a recent study that reported an unusual contact angle dependence of the bubble departure diameter [21].

The uncertainty in the measured bubble sizes is estimated to be ±0.03 mm from the pixel resolution of the images. The uncertainty in the contact angles determined from the image analyses is estimated to be <±2°. All K-type thermocouples used in the experiments are calibrated using a NIST-traceable reference Pt resistance thermometer and the uncertainty in the measured temperatures is estimated to be ±0.3 °C.

4. Results and discussion

Fig. 2 displays selected optical images of a single bubble on the superhydrophilic surface during one ebullition cycle. The equiva-

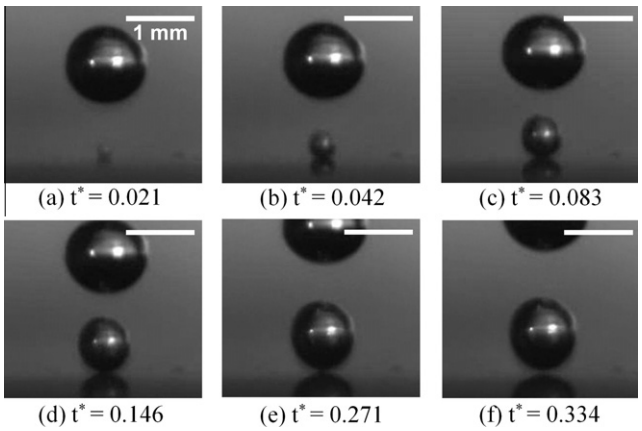

Fig. 2. Select optical images of the bubble during one ebullition cycle on the superhydrophilic surface immersed in water ($\varphi = 7.5 \pm 2°$, $\Delta T_w = 5.3$ °C, $\Delta T_{sub} = 0$–0.5 °C, $P = 1$ atm).

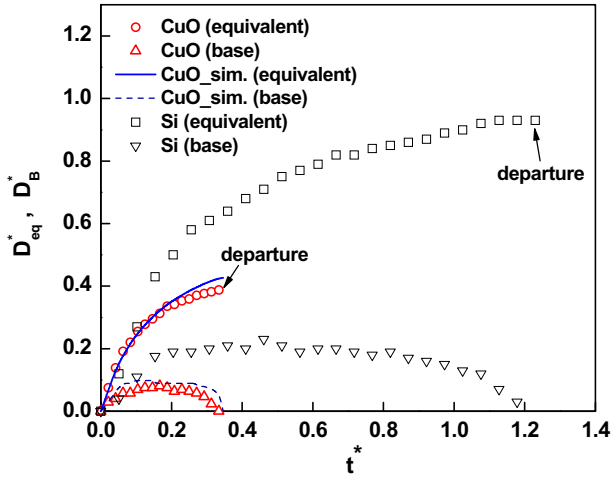

Fig. 3. Bubble growth history during one ebullition cycle on the superhydrophilic surface immersed in water ($\varphi = 7.5 \pm 2°$, $\Delta T_w = 5.3$ °C, $\Delta T_{sub} = 0$–0.5 °C) and on the silicon wafer in water ($\varphi = 44 \pm 1°$, $\Delta T_w = 4.0$ °C, $\Delta T_{sub} = 1.5$ °C).

lent and base diameters of the bubble are plotted in Fig. 3. The diameter and growth period of the bubbles are normalized using the characteristic length (l_0), velocity (u_0) and time (t_0) defined as [7]

$$l_0 = \sqrt{\frac{\sigma}{g(\rho_l - \rho_v)}}; \quad u_0 = \sqrt{g \cdot l_0}; \quad t_0 = \frac{l_0}{u_0}. \tag{1}$$

We calculate $t_0 = 1.6 \times 10^{-2}$ s and $l_0 = 2.5 \times 10^{-3}$ m for water and $t_0 = 8.7 \times 10^{-3}$ s and $l_0 = 7.4 \times 10^{-4}$ m for FC-72 at 1 atm. For comparison, the growth history of a bubble on a naturally oxidized silicon wafer from our previous study [16] is also displayed. The bubble departure diameter is observed to be ~2.5 times smaller and the growth period almost four times shorter on the present superhydrophilic surface than on the silicon surface.

The superheat required for the onset of bubble nucleation is relatively low (~5 °C) for the superhydrophilic sample with an artificial cavity. In contrast, superheat levels in excess of 20 °C are necessary to nucleate bubbles on cavity-free superhydrophilic samples. At such high superheat levels, successive bubbles merge with each other before they depart from the surface, making direct observation of single bubble dynamics not possible.

The receding contact angles measured while the bubble base is expanding are in the range of 5–7° whereas the advancing contact angles measured while the bubble base is shrinking (near the bubble departure point) range between 6° and 9°.

To confirm our experimental findings and gain further physical insight, we conduct numerical simulations under conditions comparable to those used in the experiments. Details of our numerical model were described in previous publications [7,22] and will not be repeated here. The evolution of the vapor–liquid interface is tracked using the level-set method. Simulating bubble dynamics on surfaces of contact angles <10° requires rather excessive mesh densities. To keep our computation time reasonable, we set the contact angle at 10° in our simulations. Wall temperature fluctuations are neglected, the waiting time between successive bubble nucleation is specified from the mechanistic relation [23], and changes in dynamic contact angles are ignored. Multiple evolution cycles are simulated until a quasi-steady-state is reached.

Fig. 4 shows the evolution of the bubble interface, temperature distributions, and normalized velocity vectors. ($\vec{u}^* = \vec{u}/u_0$). The simulated results are compared with the experimental observations in Figs. 3 and 4. The simulated bubble departure diameter is approximately 10% larger and the growth period is approximately 5% longer than the experimental values. The discrepancy may be explained by the slight difference in the contact angle and other approximations used in the numerical model. Overall, the simulation results are consistent with the experimental results.

In order to compare single bubble dynamics in water and in well-wetting liquids, numerical simulations are also conducted for FC-72 for the same superheat and contact angle values as the present experiments. Direct experimental comparison is difficult since well-wetting liquids require much higher superheat levels for the onset of bubble nucleation than water, introducing additional complications. Large temperature dependence of the optical properties of FC-72 and the resulting optical distortion also makes optical observation of bubbles difficult.

Fig. 5(a) compares the bubble growth history in water and in FC-72 at the same superheat (5.3 °C). The normalized bubble departure diameters D^* are comparable for both fluids, suggesting that the mechanics of bubble departure is similar. There, however, are appreciable quantitative differences in the growth kinetics and departure time, confirming that other thermophysical properties, including the thermal conductivity and the latent heat of vaporization, also play a role in single bubble dynamics. The absolute value of the bubble departure diameter is ~4 times smaller in FC-72 than in water (note that the characteristic lengthscale l_0 of FC-72 is 3.4 times smaller than that of water).

When a bubble grows on a surface, buoyancy (F_B) acts as the main upward force and the surface tension force (F_S) as the main counteracting force (see Fig. 6). The bubble departure diameter has indeed been observed to decrease with decreasing contact angle [1,5,7,8,16,17] as captured in the semi-empirical Fritz's correlation [24], which balances the buoyancy force with the surface tension force at the point of bubble departure:

$$D_d = 0.0208\varphi\sqrt{\frac{\sigma}{g(\rho_l - \rho_v)}}. \tag{2}$$

Fig. 7 plots the normalized bubble departure diameter as a function of contact angle. For the present superhydrophilic surface, the bubble departure diameter is obtained from an average over 30 ebullition cycles. The mean value is presented together with the standard deviation. To elucidate the effects of surface wettability, all the results presented in Fig. 6 are obtained at a comparable superheat levels (4–7 °C).

Fig. 7 shows that Eq. (2) predicts the bubble departure diameter reasonably well on surfaces with moderate contact angles ($\varphi = 40°$–60°). However, for superhydrophilic surfaces with contact angle < 10°, the data deviate by over 100% from the predicted value. This can be explained at least in part by differences in the shape of

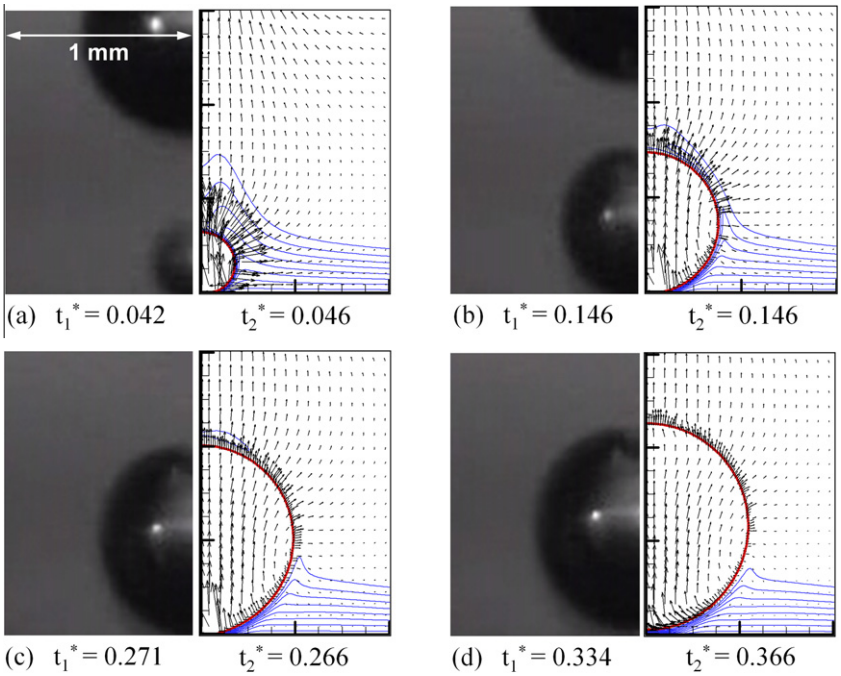

Fig. 4. Simulated bubble shapes, temperature distributions, and velocity vectors ($\varphi = 10°$, $\Delta T_w = 5.3$ °C, $\Delta T_{sub} = 0$ °C, $P = 1$ atm). t_1^* is from the experiments and t_2^* is from the numerical simulations. The isotherms correspond to 0.25–0.95 T^* where $T^* = T/\Delta T_w$.

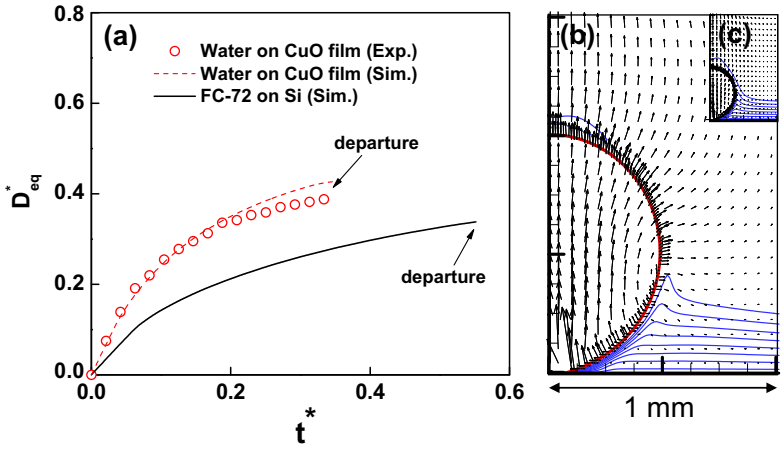

Fig. 5. (a) Bubble growth history in water and in FC-72 ($\varphi = 10°$, $\Delta T_w = 5.3$ °C, $\Delta T_{sub} = 0$ °C, $P = 1$ atm). (b) and (c) Bubble shapes, temperature distributions, and velocity vectors in water (b) at $t^* = 0.226$ and in FC-72 (c) at $t^* = 0.382$. The isotherms correspond to 0.25–0.95 T^*, $T^* = T/\Delta T_w$).

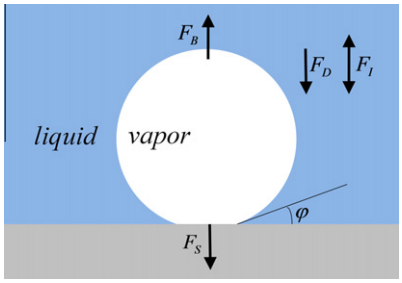

Fig. 6. Schematic representation of forces acting on a bubble growing on the wall.

bubbles close to the departure points (Fig. 8). On superhydrophilic surfaces, bubbles maintain close to a perfect spherical cap shape (Fig. 8(a)). Bubbles on surfaces with moderate contact angles, in contrast, are elongated appreciably in the vertical direction (Fig. 8(b)).

For bubbles whose shape can be modeled as a spherical cap, the buoyancy (F_B) and the surface tension force (F_S) can be expressed analytically as

$$F_B = \frac{\pi}{24} D^3 (2 + 3\cos\varphi - \cos^3\varphi) g(\rho_l - \rho_v),$$
$$F_S = \pi D \sigma \sin^2\varphi. \tag{3}$$

By equating the magnitudes of these two forces, we can estimate the departure diameter as

$$D = f(\varphi)\sqrt{\frac{\sigma}{g(\rho_l - \rho_v)}}, \quad f(\varphi) = \sqrt{\frac{24\sin^2\varphi}{(2 + 3\cos\varphi - \cos^3\varphi)}}. \tag{4}$$

Fig. 7 shows that the prediction of this analytic model matches the experimental and simulation results from the superhydrophilic surface reasonably well. The small difference may be explained by experimental uncertainties, slight non-sphericity of bubbles, and the effects of other forces.

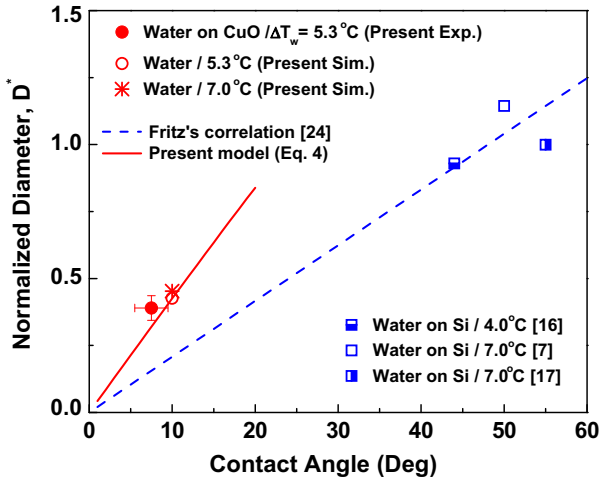

Fig. 7. The normalized bubble departure diameter as a function of the static contact angle. (ΔT_w = 4.0–7.0 °C, ΔT_{sub} = 0–1.5 °C).

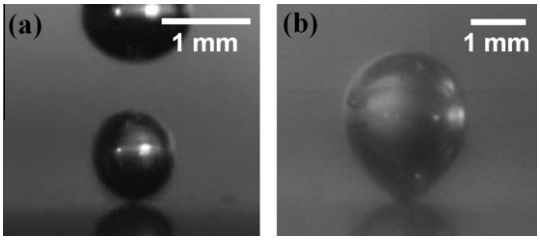

Fig. 8. Images of bubbles near the point of departure on surfaces with two different contact angles: (a) $\varphi \sim 7.5°$ and (b) $\varphi = 44°$.

Eq. (4) ignores other forces acting on the bubble, including the viscous drag (F_D) and the liquid inertia force (F_I) [15,25]. The vapor inertia force is negligible since the vapor density is much smaller than the liquid density at the atmospheric pressure. Fig. 9 compares the time evolution of each force estimated from the present numerical simulation results. In the initial stage, the bubble growth is governed by the momentum interaction between the bubble and the surrounding liquid. Consequently, the liquid inertia force has a significant effect on the growth. In the latter stage, however, the bubble growth is limited primarily by heat transfer to the

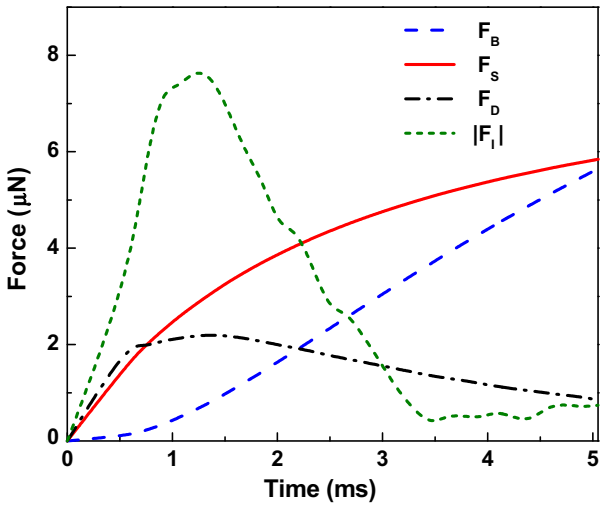

Fig. 9. Time evolution of forces acting on a simulated bubble in water during one ebullition cycle (φ = 10°, ΔT_w = 5.3 °C, ΔT_{sub} = 0 °C, P = 1 atm).

bubble interface and the effect of the momentum interaction becomes less important. The viscous drag and the liquid inertia force are estimated to be several times smaller than the buoyancy and the surface tension force near the bubble departure point.

Our past and present single bubble experiments limit wall superheat levels to 4–7 °C to prevent successive bubbles from merging with each other before they depart from the surface. This also helps elucidate the effects of surface wettability without introducing complexity associated with high wall superheat levels. Zuber [26] suggested that higher wall superheat levels result in increased departure diameters as the superheated thermal boundary layer becomes thicker with increasing superheat levels. Cole and Rohsenow [27] and Gorenflow et al. [28], in contrast, indicated that the departure diameter was independent of or only weakly depended on the wall superheat. Our recent study [29] showed that increased wall superheat does not necessarily increase the superheated thermal boundary layer thickness due to decrease in the waiting period between the ebullition cycles. The effects of wall superheat on bubble dynamics will be further discussed in our future publication.

5. Summary and conclusions

The nucleation, growth, and departure of single bubbles are studied on a superhydrophilic surface prepared by controlled chemical oxidation of a Cu film. The bubble departure diameter in water is observed to be almost ~2.5 times smaller and the growth period almost four times shorter for the superhydrophilic surface than for the oxidized hydrophilic Si surface. The bubble shapes and growth history obtained from numerical simulations agree reasonably well with the experimental results. The bubbles maintain close to a perfect spherical cap shape on the superhydrophilic surface. An approximate model based on the balance between the buoyancy and surface tension force captures the bubble departure diameter reasonably well. The nanostructuring approach and the quantitative bubble dynamics data reported in this study will help develop new surfaces for advanced heat transfer and microfluidic applications.

References

[1] V.K. Dhir, Mechanistic prediction of nucleate boiling heat transfer-achievable or a hopeless task?, J. Heat Transfer 128 (1) (2006) 1–12.
[2] Y. Takata, S. Hidaka, M. Masuda, T. Ito, Pool boiling on a superhydrophilic surface, Int. J. Energy Res. 27 (2003) 111–119.
[3] Z. Liu, Y. Qiu, Critical heat flux of steady boiling for water jet impingement in flat stagnation zone on superhydrophilic surface, J. Heat Transfer 128 (2006) 726–729.
[4] H. Kim, H.S. Ahn, M.H. Kim, On the mechanism of pool boiling critical heat flux enhancement in nanofluids, J. Heat Transfer 132 (2010) 061501.
[5] S.J. Kim, I.C. Bang, J. Buongiorno, L.W. Hu, Surface wettability change during pool boiling of nanofluids and its effect on critical heat flux, Int. J. Heat Mass Transfer 50 (2007) 4105–4116.
[6] H.S. Abarajith, V.K. Dhir, A numerical study of the effect of contact angle on the dynamics of a single bubble during pool boiling, in: Proceedings of IMECE 2002, No. IMECE2002-33876, New Orleans, LA, 2002.
[7] G. Son, V.K. Dhir, N. Ramanujapu, Dynamics and heat transfer associated with a single bubble during nucleate boiling on a horizontal surface, J. Heat Transfer 121 (3) (1999) 623–631.
[8] V.K. Dhir, H.S. Abarajith, G.R. Warrier, From nano to micro to macro scales in boiling, Microscale Heat Transfer: Fundamentals and Applications, Springer, Netherlands, 2005. pp. 197–216.
[9] N. Yaddanapudi, J. Kim, Single bubble heat transfer in saturated pool boiling of FC-72, Multiphase Sci. Technol. 12 (3–4) (2001) 47–63.
[10] S. Moghaddam, K. Kiger, Physical mechanisms of heat transfer during single bubble nucleate boiling of FC-72 under saturation conditions-I. Experimental investigation, Int. J. Heat Mass Transfer 52 (2009) 1284–1294.
[11] R. Wang, K. Hashimoto, A. Fujishima, M. Chikuni, E. Kojima, A. Kitamura, M. Shimohigoshi, T. Watanabe, Light-induced amphiphilic surfaces, Nature 388 (1997) 431–432.
[12] Y. Nam, Y.S. Ju, Comparative study of copper oxidation schemes and their effects on surface wettability, in: Proceedings of ASME IMECE 2008, No. IMECE2008-67492, Boston, MA, 2008.

[13] R.N. Wenzel, Resistance of solid surfaces to wetting by water, Ind. Eng. Chem. 28 (1936) 988–994.
[14] A.B.D. Cassie, S. Baxter, Wettability of porous surfaces, Trans. Faraday Soc. 40 (1944) 546–551.
[15] V.P. Carey, Liquid–Vapor Phase-Change Phenomena, second ed., Taylor & Francis, New York, 2008. pp. 210–211.
[16] Y. Nam, J. Wu, G. Warrier, Y.S. Ju, Experimental and numerical study of single bubble dynamics on a hydrophobic surface, J. Heat Transfer 131 (2009) 121004.
[17] D.M. Qiu, V.K. Dhir, Single bubble dynamics during pool boiling under low gravity conditions, J. Thermophys. Heat Transfer 16 (3) (2002) 336–345.
[18] R.P. Woodward, Contact Angle Measurements Using the Drop Shape Method, First Ten Angstroms Inc., Portsmouth, VA, 1999.
[19] A.F. Stalder, G. Kulik, D. Sage, L. Barbieri, P. Hoffmann, A snake-based approach to accurate determination of both contact points and contact angles, Colloid Surf. A 286 (2006) 92–103.
[20] H. Moon, S.K. Cho, Low voltage electrowetting-on-dielectric, J. Appl. Phys. 92 (2002) 4080–4087.
[21] H.T. Phan, N. Caney, P. Marty, S. Colasson, J. Gaviller, Surface wettability control by nanocoating: the effects on pool boiling heat transfer and nucleation mechanism, Int. J. Heat Mass Transfer 52 (2009) 5459–5471.
[22] J.H. Lay, V.K. Dhir, Shape of a vapor stem during nucleate boiling of saturated liquids, J. Heat Transfer 117 (1995) 394–400.
[23] C.Y. Han, P. Griffith, The mechanism of heat transfer in nucleate pool boiling, Int. J. Heat Mass Transfer 8 (1965) 887–904.
[24] W. Fritz, Maximum volume of vapor bubbles, Physik. Zeitschr. 36 (1935) 379–384.
[25] F.N. Peebles, H.J. Garber, Study on the motion of gas bubbles in liquids, Chem. Eng. Prog. 49 (1953) 88–97.
[26] N. Zuber, Hydrodynamic Aspects of Boiling Heat Transfer, US AEC Report AECU-4439, 1959.
[27] R. Cole, W. Rohsenow, Correlations of bubble departure diameters for boiling of saturated liquids, Chem. Eng. Prog. 65 (1969) 211–213.
[28] D. Gorenflow, V. Knabe, V. Bieling, Bubble density on surfaces with nucleate boiling—its influence on heat transfer and burnout heat flux at elevated saturation processes, in: Proceedings of International Heat Transfer Conference, San Francisco, 1986, pp. 1995–2000.
[29] E. Aktinol, V. K. Dhir, Numerical simulation of nucleate boiling phenomenon coupled with thermal response of the solid, in: ITT Workshop on Two-Phase Systems for Ground and Space Applications, September 27–29, Kyoto, Japan, 2010.